Analyst

Oxygen consumption rate of tumour spheroids during necrotic-like core formation

Journal:	*Analyst*
Manuscript ID	AN-ART-05-2020-000979.R1
Article Type:	Paper
Date Submitted by the Author:	30-Jun-2020
Complete List of Authors:	Mukomoto, Rei; Tohoku University, Graduate School of Environmental Studies Nashimoto, Yuji; Tohoku University, Frontier research institute for interdisciplinary sciences Terai, Takato; Tohoku University, Graduate School of Environmental Studies Imaizumi, Takuto; Tohoku University, Graduate School of Environmental Studies Hiramoto, Kaoru; Tohoku University, Graduate School of Environmental Studies Ino, Kosuke; Tohoku University, Graduate School of Engineering Yokokawa, Ryuji; Kyoto University, Department of Microengineering; Kyoto University Miura, Takashi; Kyushu Daigaku, Medical Sciences Shiku, Hitoshi ; Tohoku University, Graduate School of Engineering

SCHOLARONE™
Manuscripts

Oxygen consumption rate of tumour spheroids during necrotic-like core formation

Rei Mukomoto[1], Yuji Nashimoto[1,2,3,*], Takato Terai[1], Takuto Imaizumi[1], Kaoru Hiramoto[1], Kosuke Ino[1,3], Ryuji Yokokawa[4], Takashi Miura[5], Hitoshi Shiku[1,3,*]

[1]Graduate School of Environmental Studies, Tohoku University, Miyagi 980-8579, Japan

[2]Frontier Research Institute for Interdisciplinary Sciences (FRIS), Tohoku University, Miyagi 980-8578, Japan

[3]Graduate School of Engineering, Tohoku University, Miyagi 980-8579, Japan

[4]Department of Micro Engineering, Kyoto University, Kyoto 615-8540, Japan

[5]Graduate School of Medical Sciences, Kyushu University, Fukuoka 812-8582, Japan

Corresponding Author

* Yuji Nashimoto, e-mail: yuji.nashimoto.d8@tohoku.ac.jp,

* Hitoshi Shiku, e-mail: hitoshi.shiku.c3@tohoku.ac.jp

Abstract

Hypoxia is one of the major hallmarks of solid tumours and is associated with the poor prognosis of various cancers. A multicellular aggregate, termed a spheroid, has been used as a tumour model with a necrotic-like core for more than 45 years. Oxygen metabolism in spheroids has been studied using phosphorescence quenching and oxygen-sensitive electrodes. However, these conventional methods require chemical labelling and physical insertion of the electrode into each spheroid, which may be functionally and structurally disruptive. Scanning electrochemical microscopy (SECM) can non-invasively analyse oxygen metabolism. Here, we used SECM to investigate whether the changes of the internal structure of spheroids affect the oxygen metabolism. We investigated the oxygen consumption rate (OCR) of MCF-7 breast tumour spheroids with and without a necrotic-like core. A numerical simulation was used to describe a method for estimating the OCR of spheroids that settled at the bottom of the conventional culture plates. The OCR per spheroid volume decreased with increasing spheroid radius, indicating the limitation of the oxygen supply to the core of the MCF-7 spheroid. Formation of the necrotic-like core did not affect the oxygen metabolism significantly, implying that the core had minimal contribution to the OCR even before necrosis occurred. OCR analysis using SECM non-invasively monitors the change of oxygen metabolism in tumour spheroids. The approach is promising to evaluate various three-dimensional culture models.

Introduction

Multicellular aggregates termed spheroids are being increasingly used as a tumour model with a necrotic-like core, since they elicit more physiological cellular functions than are available in conventional monolayer culture systems[1]. Within a spheroid, there is a marked gradient of oxygen with a hypoxic region at the core, which mirrors the tumour microenvironment in the human body[2-4].

Oxygen-sensitive microelectrodes have been used since the early 1980s to measure the oxygen gradient in spheroids[5, 6]. The insertion of a microelectrode with a tip diameter of 1 ~ 5 μm in EMT6/Ro mammary carcinoma cell spheroids was successful in detecting the partial pressure of oxygen (pO_2) profile. This method was subsequently applied to other spheroids[7] and actual tissue[8]. Oxygen sensing techniques based on phosphorescence quenching[9] have created other opportunities to measure oxygen profiles in cell aggregates[10]. The synergy between phosphorescence quenching and two-photon microscopy allowed high resolution measurements of pO_2 in a deep region of a tissue[11]. Fluorescent labelling[12, 13] and electron paramagnetic resonance[14] were also developed to measure oxygen metabolism in spheroids. Although the direct measurements of pO_2 in a tissue or cell aggregates have been very promising, chemical labelling or the physical insertion of the microelectrode may disrupt cell functions in the three-dimensional environment.

While direct measurement of oxygen within spheroids has been accomplished, the oxygen profile near a spheroid with a hypoxic core has been rarely investigated[15]. Our research group has developed various electrochemical sensors to evaluate the oxygen concentration near spheroids using scanning electrochemical microscopy (SECM)[16-19], microelectrode array[20-23] and bipolar electrode[24]. The advantage of the oxygen measurement around spheroids is the non-invasive nature of the technique, which allows the sample to be used for other applications following the measurement, including implantation[16, 20, 21, 25, 26]. We previously reported the volume-dependent oxygen consumption rate (OCR) of tumour spheroids[17, 19]. However, the relationship between the

change in the internal structure of spheroids and the OCR has not been well-studied.

In this study, we investigated the OCR changes of breast tumour spheroids during the formation of a necrotic-like core. We calculated the OCR of the tumour spheroids by the electrochemical detection of the oxygen profile around the sample. Using a numerical simulation, we slightly modified the spherical diffusion theory to calculate the OCR of spheroids that settled at the bottom of a conventional flat culture dish. Comparison of OCR per spheroid volume (OCR/V) revealed that OCR/V decreased with increasing spheroid radius. Our method provides the non-invasive determination of oxygen metabolism in growing tumour spheroids. The technique is a promising approach to evaluate various three-dimensional culture models.

Materials and Methods

Cell culture, formation, and observation of spheroids

MCF-7 human breast cancer cells donated by the Cell Resource Centre for Biomedical Research (Tohoku University) were used to make tumour spheroids. The cells were cultured in RPMI 1640 (Gibco, USA) containing 10% foetal bovine serum (Gibco) and 1% penicillin streptomycin (Gibco) in a humidified incubator at 37°C with 5% CO_2. For the spheroid formation, 200 μL of the cell suspention containing 300-20,000 cells were added to each U-shaped well of 96-well plates (Sumitomo Bakelite, Japan). The spheroids were used for experiments within 7 days.

To enumerate the number of cells per spheroid, a spheroid in 10 μL of phosphate buffered saline (PBS) was transferred to 10 μL of 0.25% trypsin-EDTA (Gibco) and incubated for more than 15 min at 37°C. After dissociation of the spheroid, the number of cells was counted using the C-chip (AR BROWN, Japan).

To examine spheroid morphology, a spheroid in cell culture medium was recovered in a capillary tube (Harvard, USA). The spheroid was observed from various directions by rotating the capillary tube (Figure S1a).

Measurement of OCR by SECM

Microelectrodes were fabricated with platinum wire (φ = 20 μm) and glass capillary (World Precision Instruments, USA). Spheroids (1,250 or 10,000 cells) were prepared for measurement of the OCR using the HV-405 SECM system (Hokuto Denko, Japan). The experiment was performed in a 35 mm diameter culture dish (Falcon, USA) filled with 3 mL of embryo respiration assay medium - 2 (Research Institute for the Functional Peptides, Japan). The culture dish was set on a hot plate (setting temperature: 25°C, actual temperature: 21°C; Tokai Hit, Japan) on the microscope stage. The XYZ stage and potentiostat were controlled using HV-405 SECM system. An oxygen profile was obtained by scanning the platinum disk microelectrode vertically for

500 μm near the spheroid at −0.5 V vs. Ag/AgCl. The up-and-down scan was repeated three times with a scan speed of 30 μm/s (Figure 1) and the oxygen reduction current was measured. The oxygen concentration near a spheroid, C, was calculated according to the spherical diffusion theory[18] as:

$$C = \frac{(C_s - C^*)r_s}{L_0} + C^* \qquad (1)$$

where r_s is the radius of the spherical sample, and C_s and C^* are the concentrations of oxygen at the sample surface and in the bulk fluid, respectively. In this study, the distance from the centre of the spherical sample (L_0) is expressed as:

$$L_0 = \left[z^2 + r_s^2\right]^{0.5} \quad (2)$$

where z is the scanning distance from the side of a spheroid. r_s/L_0 goes 0 when the microelectrode is far from the surface of the spheroid, and approaches 1 when the microelectrode is near. From equation (1), C^* and C_s were determined from the intercepts at $r_s/L_0 = 0$ and 1, respectively. The total OCR of the sample (mol/s) are given as follows:

$$\mathrm{OCR} = 4\pi r_s D \Delta C \qquad (3)$$

where D is the diffusion coefficient of oxygen, and ΔC is the difference between the bulk and the sample surface ($\Delta C = C^* - C_s$). ΔC was electrochemically determined using $C^* = 2.10 \times 10^{-7}$ mol/cm^3. OCR was calculated using $D = 2.10 \times 10^{-5}$ cm^2/s and equation (3)[27].

Histological analysis

Spheroids were removed from the wells and fixed with 4% paraformaldehyde (Alfa Aesar, USA) in PBS for histological analysis. The spheroids were sequentially transferred to 10, 15 and 20% solutions of sucrose (Wako, Japan) in PBS and kept for several hours. The spheroids were embedded in Tissue-Tek Cryomold (Sakura Finetek, Japan) filled with optimum cutting temperature compound (Sakura Finetek) and frozen in liquid nitrogen. Each frozen sample was

sectioned with a thickness of 10 μm using a model CM1520 cryostat (Leica, Germany) and air-dried on a glass slide (Matsunami Glass Ind., Ltd, Japan) for 30 min. Nuclei and cytoplasm were stained with haematoxylin and eosin using a commercially available kit (ScyTek Laboratories, USA).

Imaging and statistical analysis

Phase contrast images were captured using a model IX71 inverted microscope (Olympus, Japan) equipped with ×4, ×10, ×20 and ×40 lenses, and a model DP71 CCD camera (Olympus, Japan). The images were stored using DP controller software (Olympus). For the histological analysis, the images were recorded using an Eclipse Ts2 inverted microscope (Nikon, Japan) and MIchrome 20 colour CCD camera (Tucsen Photonics, China). Spheroid sizes were determined from the phase contrast images using Fiji image processing software (National Institutes of Health, USA)[28]. In the determination, r_s was calculated as: $r_s = 0.5^2(a + b)$, where a and b are the major and minor axis of a spheroid, respectively. Volume (V) was also calculated according to the equation: $V = (4/3)\pi r_s^3$. The number of samples are specified in each figure caption.

Numerical simulation of oxygen concentration

The oxygen profile surrounding a spheroid was simulated by two-dimensional axisymmetric modelling using Multiphysics ver. 5.4 (COMSOL Inc., USA). The plate condition was defined as when the spheroid was settled at the bottom of a cylindrical vessel with a radius and height of 17.5 mm, and the radius of the spheroid was set as 93, 185 and 370 μm in the simulation. The initial concentration of oxygen in the area, including the diffusion coefficient of oxygen in the solution and in the spheroid, were 2.10 $\times 10^{-7}$ mol/cm^3, 2.10 $\times$ 10^{-5} cm^2/s, and 1.65 $\times$ 10^{-5} cm^2/s, respectively[27, 29]. The spheroid was assumed to consume oxygen at 4.18 $\times$ 10^{-3} mol/(s·m^3)[17]. The oxygen profiles near a spheroid floating in solution (8.75 mm above the bottom of the cylindrical

vessel, which was defined as the floating condition) and in the inverted cone-shaped microwell (radius and height of 17.5 mm, defined as cone-shaped well) were also simulated in the identical condition.

Results

Preparation of tumour spheroid with a necrotic-like core

Initially, we investigated the culture conditions of the MCF-7 spheroids to obtain individual spheroids having a necrotic core. Phase contrast images of MCF-7 spheroids with an initial cell number of 300, 625, 1,250, 2,500, 5,000, 10,000, and 20,000 cells/well are shown in Figure 2a. After 2 days in suspension culture, a black core appeared at the centre of the spheroids with an initial cell number exceeding 5,000 cells/well. Figure 2b shows the relationship between spheroid radius and the black core for 1,250 and 10,000 cells/well. The threshold radius for development of the black core in MCF-7 spheroids was 260 μm. Until day 6, spheroids initially comprising 1,250 cells/well had a radius <260 μm and no black core. The radius of spheroids comprising 1,250 cells/well became larger in a time-dependent manner and exceeded 260 μm at day 7. These spheroids also developed a black core. Spheroids comprising 10,000 cells/well had a radius >260 μm and developed black cores after day 1. The radius of the black cores became larger when the spheroids became bigger in both conditions. Interestingly, for spheroids with a radius exceeding 260 μm, the radius of the black core depended on the radius of the spheroid and not on the culture period or the initial cell number (see 1,250 cells/well and day 7 and 10,000 cells/well on day 2 in Figure 2). The other culture conditions (initial cell concentrations of 20,000, 5,000, 2,500, 625 and 300 cells/well) displayed the same correlation between the radii of the spheroids and the black core, except for 20,000 cells/well at day 1 (Supplementary Table S1).

To confirm whether the black core showed typical features of necrosis, such as fragmentation of nucleus, spheroids were sectioned and histologically evaluated (Figure 2c). When the initial cell concentration was 10,000 cells/well, spheroids that each displayed a black core after 5 days in suspension culture showed a double-layer structure (Figure 2c). The cell concentration was less in the black core than in the outer layer. The double-layer structure was not observed in spheroids lacking a black core (Figure 2c, 1,250 cells/well). The nuclei in the black core were

smaller than those in the outer layers and in the condition of 1,250 cells/well. This finding implied that pyknosis, which is one of the changes in the nucleus that occurs during necrosis, occurred at the core. The cell number per spheroid was plotted with respect to the volume of the spheroid in Supplementary Figure S2. The exponential part of the power function approximation trendline was <1, whereas the exponential part became close to 1 when plotted with the volume after removing the black core. These findings indicated that the number of cells per unit volume became constant, except in the area of the black core, implying that the black core contained few live cells. The collective results defined the black core as a necrotic-like core.

We selected MCF-7 spheroids prepared with 1,250 and 10,000 cells/well as spheroids without and with a necrotic-like core, respectively. Figure S1b shows the morphologies of the spheroids prepared with 1,250 and 10,000 cells/well. In both culture conditions, the MCF-7 spheroids maintained their spherical shape for 7 days in suspension culture. This permitted the analysis of the OCRs of the spheroids using the spherical diffusion theory as detailed next.

Simulation of oxygen concentration for spherical diffusion analysis

The simulated oxygen concentration profiles near spheroids with radii of 370 μm decreased (Figure 3a) owing to the oxygen consumption of the spheroids. The shape of the oxygen profile was close to hemispherical in the plate condition and spherical in the floating condition. The oxygen profile near the spheroid was lower in the plate condition that in floating condition (Figure 3b). Spheroids having smaller radii of 93 and 185 μm showed a similar trend (Supplementary Figures S3a and S3b). The oxygen concentration at the contact side of the spheroids in the plate condition was substituted for C_s in equation (3) and the OCRs were calculated (Table 1). The calculated OCRs in the floating condition corresponded to the input values, whereas those in plate condition were 41.0 - 45.3% higher. The deviation in the plate condition was likely derived from the plate substrate at the bottom. Since the oxygen diffusion at the bottom side was hindered by the plate

substrate, the oxygen profile at the top side should partially reflect the OCR of the bottom side of the spheroid, suggesting the need for the correction of equation (3). From Table 1, the correction factor was calculated as follows:

$$\frac{\mathrm{OCR(Floating)}}{\mathrm{OCR(Plate)}} = 0.69$$

Equation (3) was modified by multiplying the correction factor (0.69) as follows:

$$\mathrm{OCR_{plate}} = 2.76\pi r_s D\Delta C \quad (4)$$

Equation (4) provided almost same OCRs as the inputs for other spheroid radii (Table 1). Hereafter, equation (4) was used for the calculation of the OCR in the study.

Radius-dependent OCR

We compared the OCRs of MCF-7 spheroids comprising 1,250 and 10,000 cells from day 1 to day 7 in the suspension culture (Figure 4a). The OCRs of the MCF-7 spheroids increased in a temporal manner for both cell concentrations, consistent with increasing spheroid dimeter (Figure 2b). Figure 4b summarises the change of OCR/V depending on the radius. Until day 4, for both 1,250 and 10,000 cells/well conditions, OCR/V increased as the radius became larger. On the contrary, after 4 days in suspension culture, OCR/V showed a downward trend when the radius increased. Interestingly, after day 4, OCR/V in the 1,250 and 10,000 cells/well conditions showed a similar downward trend. We confirmed that the OCR/V in the other culture conditions of an initial cell density of 300, 625, 2,500, 5,000 and 20,000 cells/well displayed the same decreasing line after 3 days in suspension culture (Supplementary Figure S4). No significant change was evident on the day when necrotic-like cores appeared in the spheroids (day 7 in 1,250 cells/well condition and day 2 in 10,000 cells/well condition, Figure 4b).

Discussion

Oxygen is an essential molecule, particularly in biological samples containing respiring cells and tissues. As the key metabolite and the energy source in tissues, oxygen is used to produce adenosine triphosphate (ATP) through the electron transport chain and oxidative phosphorylation. In addition, cells sense oxygen concentration by mechanisms like the hypoxia-inducible factor (HIF) pathway and modulate gene expression levels to adapt to hypoxia. Spheroid culture uses oxygen gradients in spheroids to recapitulate avascular tumour growth. Although a number of previous studies reported oxygen sensing methods within spheroids, most of the methods require chemical labelling or physical insertion of the sensors in the spheroids, which might disturb the functions or structure of the spheroids. In this study, we investigated whether OCRs calculated from the oxygen profile near individual spheroids could reflect the hypoxic condition within each spheroid.

Formation of a necrotic-like core in MCF-7 spheroids

We used MCF-7 cells to model tumour spheroids with and without a necrotic-like core. Cryosections of MCF-7 spheroids prepared using 10,000 cells/well as the initial cell seeding condition revealed smaller nuclei at the core than those in the outer layer (Figure 2c), indicating that necrotic pyknosis in the core. A previous study reported that the HIF-2α and lactate dehydrogenase A markers of hypoxia were strongly expressed in the core, supporting the existence of an oxygen gradient in the MCF-7 spheroids[30]. A thin, cell-free area appeared at the interface between the necrotic core and outer layer (Supplementary Figure S5). This cell-free area was also observed in previous studies and was identified as the poly (ADP-ribose) polymerase-1 positive ($PARP\text{-}1^{+}$)[31] and light chain 3B positive ($LC3B^{+}$)[32] area (apoptotic area). The previous studies demonstrated that the apoptosis of the interface was one step in formation of acini. Collectively, the MCF-7 spheroids constructed in this study had a necrotic-like core surrounded by a thin apoptotic layer.

OCR calculation in plate condition

Using the numerical simulation (Figure 3), we modified equation (3) to precisely calculate the OCRs of the spheroid in plate condition (equation (4)). The calculated OCRs in the plate condition using equation (4) gave consistent values with those in the floating condition as calculated using equation (3) and in the cone-shaped microwell system used in our previous study[19] (Table 1 and Supplementary Figure S6a). Of note, in this study, we just simulated the change of the oxygen profile depending on the geometries of the three type of culture plates (floating, plate, and cone-shaped microwell). We did not consider the change of cell activities due to the change of culture plates. Indeed, another correction factor was needed for the comparison between the floating condition and the cone-shaped microwell to correct the change of OCRs[12,33]. Supplementary Figure S6b shows the comparison between calculated OCRs in this study (equation (4), 21°C) and in our previous study using cone-shaped microwell[19] (equation (5) in Supplementary Figure S6a, 37°C). Although the temperature during OCR measurement greatly affected the OCRs and measurements conducted at 37°C yielded higher OCRs than the values obtained at room temperature[27], the OCRs in this study corresponded fairly well with those in the previous study. This result implies that the cell activities in the plate condition were higher than in the cone-shaped microwell because the temperature for OCR measurement in this study (21°C) was lower than in the previous studies (37°C). Future studies should include the determination of the correction factor for the change of cell activities in same experimental condition, including the temperature.

Size-dependent OCR/V during formation of a necrotic-like core

Analysis of the oxygen profile near spheroids revealed that OCR/V decreased with increasing spheroid radius (volume) after 4 days in suspension culture (Figure 4b). Direct insertion of an oxygen-sensitive microelectrode in spheroids previously revealed a similar decrease of

OCR/V with increasing spheroid radius[7]. The decreased OCR/V likely reflected the limited oxygen supply to the core. Presently, when the necrotic-like core was formed in a spheroid, the OCR/V decreased in both culture conditions (from day 6 to day 7 in the 1,250 cells/well condition and from day 1 to day 2 in the 10,000 cells/well condition, Figure 4b). However, the decrease was not as large and still displayed the same downward trend line for the OCR/V before the formation of the necrotic-like core (from day 4 to day 6 in the 1,250 cells/well condition). The findings implied that the centre region where the necrotic-like core formed did not contribute substantially to the OCR, even before the appearance of the necrotic-like core. Interestingly, we also observed the increase of OCR/V until 4 days in suspension culture, which was not seen in the previous studies[7, 19]. The increases of OCR/V were observed in both the 1,250 and 10,000 cells/well conditions, implying that the oxygen metabolism of the MCF-7 cells was low just after spheroid formation and gradually recovered thereafter. Thus, OCR/V provides biological information during the formation of spheroids and the necrotic-like core.

Conclusion

We investigated whether SECM could non-invasively monitor the change of OCRs of tumour spheroids during the formation of a necrotic-like core. MCF-7 spheroids with and without the necrotic-like core were successfully prepared using a 96-well plate. The novel method permits the precise determination of OCRs of tumour spheroids, similar to our previously described cone-shaped microwell method. OCR/V decreased with increasing spheroid radius, indicating the development of the necrotic-like core in the MCF-7 spheroids. The non-invasive determination of OCR by SECM permits the analysis of cellular metabolism in tumour spheroids. In addition, we numerically simulated the difference between the methods of OCR measurement by SECM and updated the equation to calculate OCR in plate condition, which is the first attempt as far as we know. This method will be useful because it is important to retain the structures intact in three-dimensional culture models including organoids.

Acknowledgements

This work was supported by the Japan Society for the Promotion of Science (JSPS) KAKENHI (Grant numbers 18H01999, 18H01840 and 19K20658) and Grant-in-Aid for JSPS Fellows (Grant number 20J21401), CREST JST (Grant Number JPMJCR14W4), and The Asahi Glass Foundation, Research Grant from the Nakatomi Foundation. We extend our appreciation to Prof. Kenshiro Hara, Graduate School of Agriculture, Tohoku University, for his help with the cryo-section experiment.

Author contributions

R.M. performed the experiments. R.M. and Y.N. performed data analyses. R.M., Y.N. and T.I. wrote the macro for the calculation of spheroid radius. Y.N. and H.S. conceived and designed the project. K.I., Y.N., and R.M. performed the numerical simulation. R.M., Y.N., T.T., T.I., K.H., K.I., R.Y., T.M., and H.S. wrote the manuscript.

References

1. E. Fennema, N. Rivron, J. Rouwkema, C. van Blitterswijk and J. de Boer, *Trends Biotechnol.*, 2013, **31**, 108-115.
2. F. Hirschhaeuser, H. Menne, C. Dittfeld, J. West, W. Mueller-Klieser and L. A. Kunz-Schughart, *J. Biotechnol.*, 2010, **148**, 3-15.
3. R. M. Sutherland, *Science*, 1988, **240**, 177-184.
4. R. M. Sutherland, J. A. McCredie and W. R. Inch, *JNCI, J.Natl.Cancer Inst.*, 1971, **46**, 113-120.
5. W. F. Mueller-Klieser and R. M. Sutherland, *Br. J. Cancer*, 1982, **45**, 256-264.
6. W. F. Mueller-Klieser and R. M. Sutherland, *Cancer Res.*, 1982, **42**, 237-242.
7. L.A. Kunz-Schughart, J. Doetsch, W. Mueller-Klieser and K. Groebe, *Am.J.Physiol.:Cell Physiol.*, 2000, **278**, C765-C780.
8. R. D. Braun, J. L. Lanzen, S. A. Snyder and M. W. Dewhirst, *Am.J.Physiol.:Heart Circ.Physiol.*, 2001, **280**, H2533-H2544.
9. W. L. Rumsey, J. M. Vanderkooi and D. F. Wilson, *Science*, 1988, **241**, 1649-1651.
10. R. I. Dmitriev and D. B. Papkovsky, *Cell. Mol. Life Sci.*, 2012, **69**, 2025-2039.
11. S. Sakadzic, E. Roussakis, M. A. Yaseen, E. T. Mandeville, V. J. Srinivasan, K. Arai, S. Ruvinskaya, A. Devor, E. H. Lo, S. A. Vinogradov and D. A. Boas, *Nat. Methods*, 2010, **7**, 755-759.
12. D. R. Grimes, C. Kelly, K. Bloch and M. Partridge, *J.R.Soc.,Interface*, 2014, **11,** 20131124.
13. M. L. Woods, C. J. Koch and E. M. Lord, *Int. J. Radiat. Oncol., Biol., Phys.*, 1996, **34**, 93-101.
14. L. M. Langan, N. J. F. Dodd, S. F. Owen, W. M. Purcell, S. K. Jackson and A. N. Jha, *PLoS One*, 2016, **11**, e0149492.
15. S. C. Lesher-Perez, G.-A. Kim, C.-H. Kuo, B. M. Leung, S. Mong, T. Kojima, C. Moraes, M. D. Thouless, G. D. Luker and S. Takayama, *Biomater. Sci.*, 2017, **5**, 2106-2113.
16. H. Shiku, T. Shiraishi, H. Ohya, T. Matsue, H. Abe, H. Hoshi and M. Kobayashi, *Anal. Chem.*, 2001, **73**, 3751-3758.
17. Y. S. Torisawa, A. Takagi, H. Shiku, T. Yasukawa and T. Matsue, *Oncol. Rep.*, 2005, **13**, 1107-1112.
18. T. Yasukawa, I. Uchida and T. Matsue, *Biophys. J.*, 1999, **76**, 1129-1135.
19. Y. Zhou, T. Arai, Y. Horiguchi, K. Ino, T. Matsue and H. Shiku, *Anal. Biochem.*, 2013, **439**, 187-193.
20. Y. Date, S. Takano, H. Shiku, K. Ino, T. Ito-Sasaki, M. Yokoo, H. Abe and T. Matsue, *Biosens. Bioelectron.*, 2011, **30**, 100-106.
21. K. Hiramoto, M. Yasumi, H. Ushio, A. Shunori, K. Ino, H. Shiku and T. Matsue, *Anal. Chem.*, 2017, **89**, 10303-10310.
22. K. Ino, M. Sen, H. Shiku and T. Matsue, *Analyst*, 2017, **142**, 4343-4354.
23. Y. Kanno, K. Ino, H. Abe, C. Sakamoto, T. Onodera, K. Y. Inoue, A. Suda, R. Kunikata, M.

Matsudaira, H. Shiku and T. Matsue, *Anal. Chem.*, 2017, **89**, 12778-12786.

24. K. Ino, R. Yaegaki, K. Hiramoto, Y. Nashimoto and H. Shiku, *ACS sensors*, 2020, **5** 740-745.
25. H. Kurosawa, H. Utsunomiya, N. Shiga, A. Takahashi, M. Ihara, M. Ishibashi, M. Nishimoto, Z. Watanabe, H. Abe, J. Kumagai, Y. Terada, H. Igarashi, T. Takahashi, A. Fukui, R. Suganuma, M. Tachibana and N. Yaegashi, *Hum. Reprod.*, 2016, **31**, 2321-2330.
26. T. Maezawa, M. Yamanaka, S. Hashimoto, A. Amo, A. Ohgaki, Y. Nakaoka, A. Fukuda, T. Ikeda, M. Inoue and Y. Morimoto, *J. Assist. Reprod. Genet.*, 2014, **31**, 1099-1104.
27. H. Shiku, Y. Torisawa, A. Takagi, S. Aoyagi, H. Abe, H. Hoshi, T. Yasukawa and T. Matsue, *Sens. Actuator B-Chem.*, 2005, **108**, 597-602.
28. J. Schindelin, I. Arganda-Carreras, E. Frise, V. Kaynig, M. Longair, T. Pietzsch, S. Preibisch, C. Rueden, S. Saalfeld, B. Schmid, J. Y. Tinevez, D. J. White, V. Hartenstein, K. Eliceiri, P. Tomancak and A. Cardona, *Nat. Methods*, 2012, **9**, 676-682.
29. Y. Jiang, J. Pjesivac-Grbovic, C. Cantrell and J. P. Freyer, *Biophys. J.*, 2005, **89**, 3884-3894.
30. E. J. Jarman, C. Ward, A. K. Turnbull, C. Martinez-Perez, J. Meehan, C. Xintaropoulou, A. H. Sims and S. P. Langdon, *Breast Cancer Res.*, 2019, **21**, 10.
31. A. P. Andersen, M. Flinck, E. K. Oernbo, N. B. Pedersen, B. M. Viuff and S. F. Pedersen, *Mol. Cancer*, 2016, **15**, 45.
32. J. B. do Amaral, P. Rezende-Teixeira, V. M. Freitas and G. M. Machado-Santelli, *Tissue Eng., Part C*, 2011, **17**, 1097-1107.
33. H. Shiku, T. Shiraishi, S. Aoyagi, Y. Utsumi, M. Matsudaira, H. Abe, H. Hoshi, S. Kasai, H. Ohya and T. Matsue, *Anal. Chim. Acta*, 2004, **522**, 51-58.

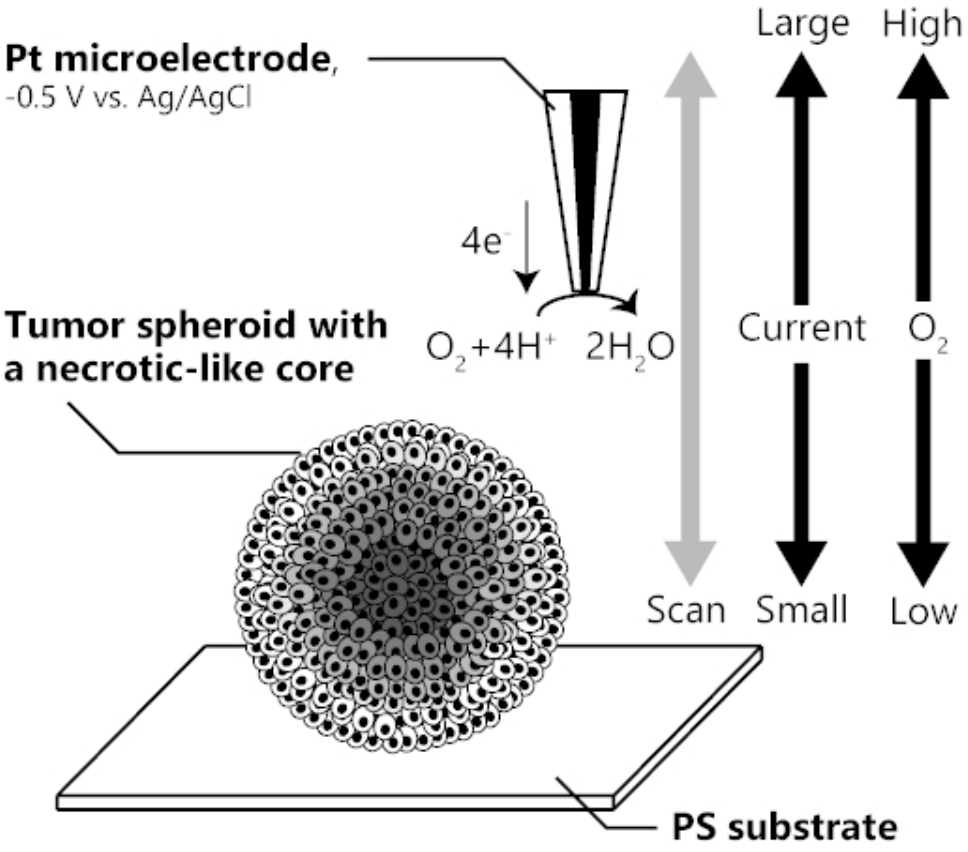

Figure 1: Schematic of the OCR measurement using SECM. A platinum (Pt) microelectrode was scanned from the side of the tumour spheroid to 500 μm above the spheroid lineally. Scanning was repeated three times for each measurement. The oxygen profile around the spheroids can be obtained by calculating the oxygen concentration from the oxygen reduction current. In the vicinity of the spheroid, the oxygen reduction current was decreased owing to the respiration activity of the spheroid.

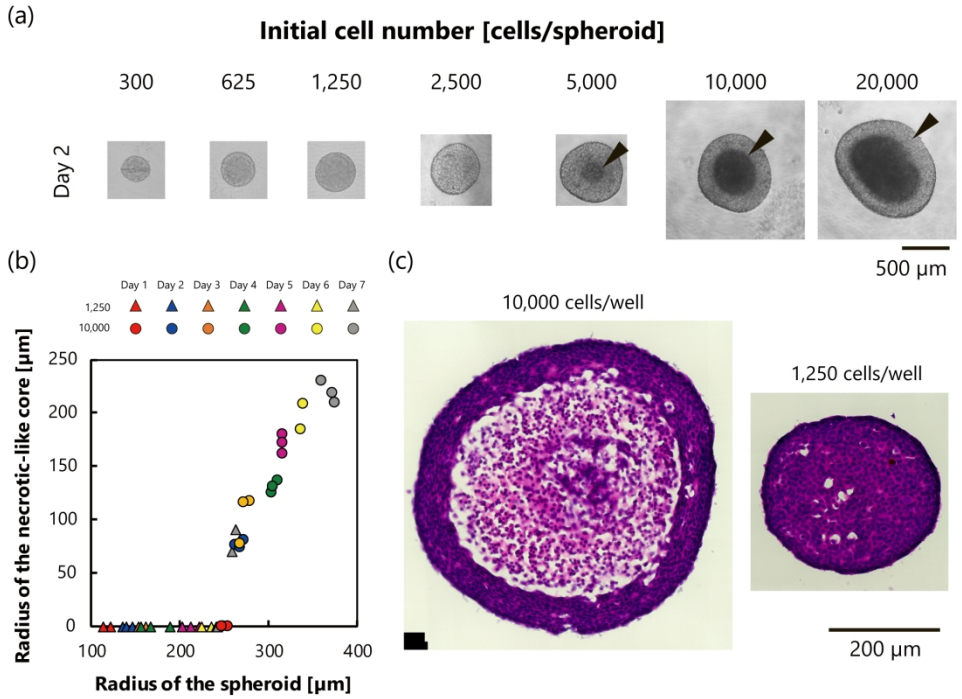

Figure 2: Investigation of the culture condition to acquire an MCF-7 spheroid with a necrotic-like core. (a) Phase contrast images of MCF-7 spheroids after 2 days in suspension culture. Black arrow heads indicate black cores formed in the MCF-7 spheroids. The scale bar is for all images in (a). (b) The relationship between a spheroid radius and a black core for 1,250 and 10,000 cells/well spheroids (n = 3 for each culture condition). (c) Tile scan of cryosections of MCF-7 spheroids after 5 days in suspension culture (1,250 and 10,000 cells/well). Red indicates cytoplasm (stained with eosin) and purple indicates nuclei (stained with haematoxylin).

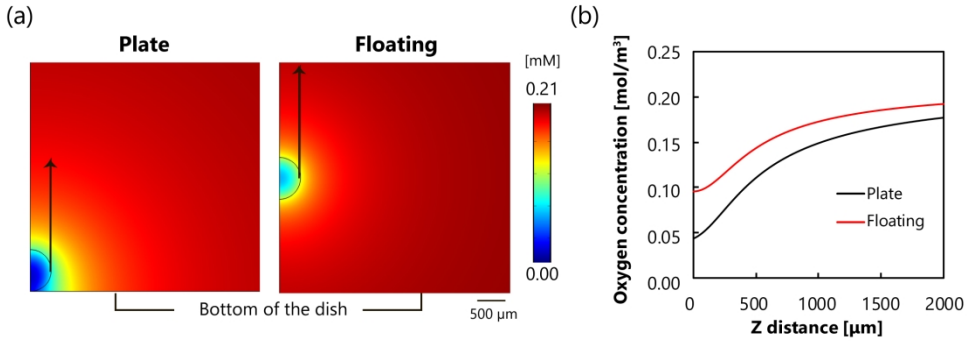

Figure 3: Numerically simulated oxygen profile near a spheroid. (a) Left: plate condition, right: floating condition. Black arrows represent the z direction. (b) Line plot of the oxygen concentration corresponding to the black arrows in (a). The spheroid radii were 370 μm in the plate and floating conditions.

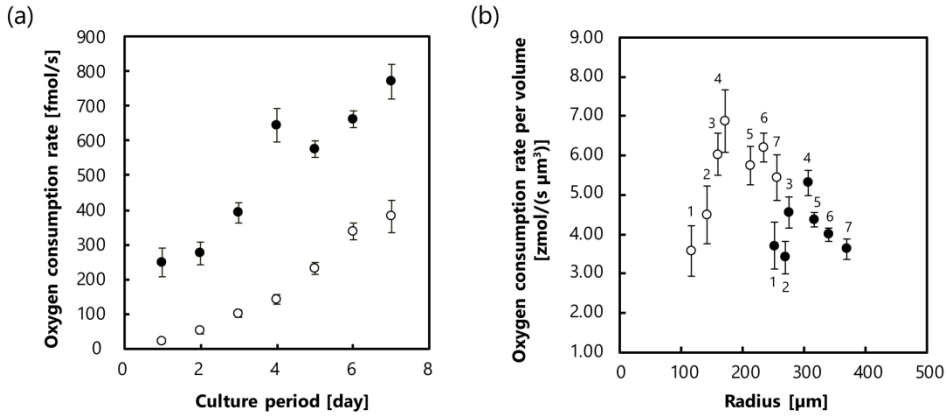

Figure 4: Time course change of the oxygen consumption rates (a) per spheroid and (b) per volume. Filled circles: 10,000 cell/well, open circles: 1,250 cells/well. Numbers in (b) represent culture days in suspension (n = 3 for each culture condition).

r_s [μm]		93	185	370
Input [fmol/s]		14.1	112.6	886.4
Floating	OCR [fmol/s]	13.9	108.9	859.9
	Δ [%]	1.6	3.3	3.0
Plate	OCR [fmol/s]	20.1	157.8	1247.6
	Δ [%]	42.8	40.2	40.7
Plate (equation (4))	OCR [fmol/s]	13.9	108.9	860.8
	Δ [%]	1.5	3.3	2.9
Cone-shape (equation (5a) in Supplemetary information)	OCR [fmol/s]	14.1	109.7	—
	Δ [%]	0.1	2.6	—

Table 1: Calculated oxygen consumption rates and deviation from the input value. Oxygen consumption rates (OCRs) in floating and plate conditions were derived from calculations. Equation (4) successfully corrected the deviation in plate condition. Input and Δ were calculated as $4.18 \times 10^{-3}/(4/3\pi r_s^3)$ and |Input-OCR|/Input × 100, respectively.

131x76mm (150 x 150 DPI)